Tellus (1977), *29*, 393–401

Kinematic analyses over eastern Asia during a subperiod of the air mass transformation experiment 1975

By YI-TSUEI PAI SHEU and PHILLIP J. SMITH, *Department of Geosciences, Purdue University, West Lafayette, Indiana 47907, U.S.A.*

(Manuscript received September 20; in final form December 13, 1976)

ABSTRACT

This study examines the large-scale vorticity and vertical motion fields over eastern Asia during a subperiod (13–16 February) of the Air Mass Transformation Experiment (AMTEX) 1975. This represents a period of cyclogenesis and subsequent formation of mesoscale cellular convection (MCC) over the AMTEX region.

Vertical motion and vorticity fields reflect the developing cyclone and a short synoptic-scale upper wave which propagated across the computational region. Results for the AMTEX region reveal that during MCC occurrences large-scale downward motion and a change from negative to positive vertical gradient of vorticity in the lower troposphere occur.

1. Introduction

Meteorological satellite cloud photography, as first reported by Krueger & Fritz (1961), has shown surprisingly organized mesoscale convective clouds over vast regions of the ocean. The existence of these mesoscale cellular convection (MCC) patterns in the atmosphere suggests a scale of convection that is significant to air–sea energy exchange mechanisms. The study of many observational cases by Hubert (1966) shows that these cloud formations commonly occur as "open" and "closed" cells. Open cells are characterized by approximately hexagonal clear areas surrounded by cloud walls, while closed cells occur as hexagonal cloud-covered areas surrounded by walls of clear air. A comprehensive summary of the physical and geometrical features of these two cell classes is given in Agee & Dowell (1974), while a general review of MCC is found in Agee et al. (1973).

These mesoscale events are influenced by and in turn exert influence on the synoptic-scale circulations. One approach to studying these influences is through diagnostic analyses of the large-scale kinematics for an area encompassing the relevant large-scale and mesoscale processes. The utility of kinematic parameters, particularly vorticity and vertical motion, for diagnosing individual synoptic-scale circulation systems has been widely recognized for many years (see, for example, Miller & Panofsky, 1958; Newton & Palmen, 1963; O'Neill, 1966; Krishnamurti, 1968; Smith, 1971; Chien & Smith, 1973).

One of the common regions for mesoscale cellular convection is east of the Asian continent in association with strong cold air advection following the passage of a winter extratropical cyclone over the East China Sea in the vicinity of the Kuroshio Current. Because of the prominent convective activity in this region, it was chosen for an experiment in which energy and momentum exchanges between the sea surface and its overlying air mass would be intensively studied. This experiment, planned by the Japanese Committee for GARP and known as the Air Mass Transformation Experiment (AMTEX), provided for extensive surface and upper air data collections for two-week periods in February of 1974 and 1975.

The present study is concerned with analyses of synoptic-scale vorticity and vertical motion fields over an area encompassing and extending upstream from the AMTEX region for the period 13–16

February 1975. This is a subperiod of the 1975 AMTEX during which cyclogenesis and subsequent formation of MCC occurred over the AMTEX region.

2. Computational aspects

A. *Data and study area*

Data used in this study were rawinsonde observations (0000 and 1200 GMT) for the period 0000 GMT 13 February through 1200 GMT 16 February 1975. Wind, temperature, and geopotential height data were available at the mandatory pressure levels of surface, 1000 mb, 850 mb, 700 mb, 500 mb, 400 mb, 300 mb, 250 mb, 200 mb, 150 mb, and 100 mb. Missing data were estimated either by a linear interpolation in the vertical direction or by a distance-weighted horizontal interpolation developed by Chien and Smith (1973). The areal depictions of synoptic, vertical motion, and vorticity patterns utilize data from the stations shown in Fig. 1. The spatial distribution of AMTEX stations is comparable to that in Japan and eastern China. Detailed analyses of the kinematic features are restricted to the circled stations in the AMTEX region (hexagonal network in Fig. 1).

In the AMTEX network upper air observations were made four times daily at five out of eight stations. However, in order to provide identical temporal coverage for all stations in the study region, twice daily data were used in the present analyses. This insures that both the AMTEX stations and those external to the AMTEX region are representative of the same spatial and temporal scales, which are similar to those defined for the synoptic scale by Fiedler & Panofsky (1970).

B. *Computing procedures*

The derivatives of the wind components, required for the calculations of horizontal velocity divergence and vertical component of vorticity, were obtained using the two-dimensional, second-order Taylor's series procedure described by Chien & Smith (1973). This method involves the series expansion of the two wind components about any arbitrary data station utilizing wind information from five surrounding stations to produce a system of five linear equations with the two first-order and three second-order derivatives as unknowns. The advantages of schemes such as this, which account for non-linear variations in the wind field, are noted by Chien & Smith and Schmidt & Johnson (1972). Of course no scheme can completely eliminate error components. However,

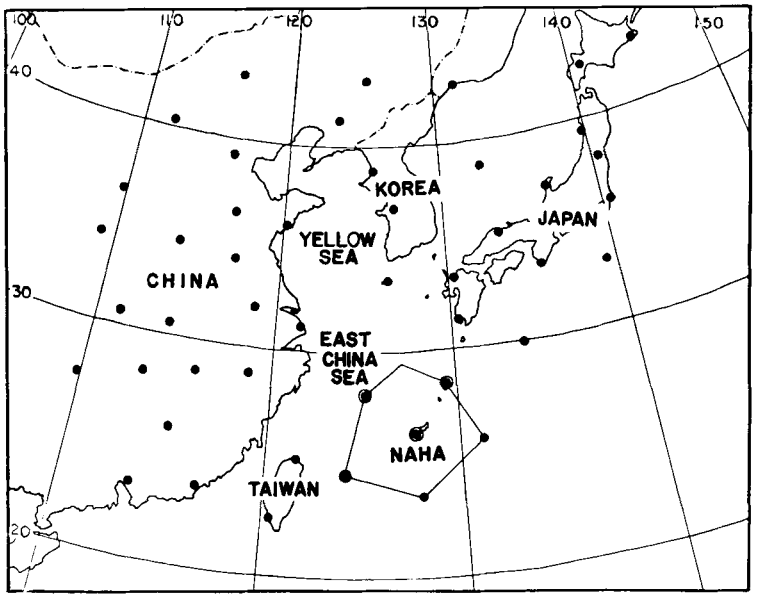

Fig. 1. Rawinsonde data stations. AMTEX network identified by hexagonal region.

as noted by Chien & Smith, vorticity fields appear to be quite representative of synoptic-scale horizontal flow, while divergence fields contain systematic errors which can be reduced using adjustment algorithms such as those proposed by O'Brien (1970).

Vertical motions were computed by the kinematic method. Cumulative-bias errors in vertical motions were adjusted using a scheme suggested by O'Brien (1970) and applied by Fankhauser (1969), Smith (1971), and Chien & Smith (1973), with imposed vertical boundary conditions of $\omega = 0$ at the surface and 100 mb. Each parameter was calculated directly at each station, level, and observation time.

In order to reduce the errors caused by random instrumental errors and non-representative atmospheric perturbations, a vertical filtering technique proposed by Danielsen (1959) was used to smooth the raw wind data. The horizontal wind components were filtered by a three-point binomial smoothing scheme given by

$$u'_i = \frac{u_{i-1} + 2u_i + u_{i+i}}{4} \qquad (1)$$

$$v'_i = \frac{v_{i-1} + 2v_i + v_{i+1}}{4}$$

where i is the level indicator, u and v are components of wind speed in the x and y direction respectively, and u' and v' are filtered wind components. As seen in the examples provided in Fig. 2, vertically filtered wind profiles remain very similar to those of the unfiltered wind, demonstrating a smoother vertical distribution without significant change in the speed and direction.

3. Synoptic discussion

The primary surface weather features at the beginning of the study period consisted of a cyclone developing southwest of the AMTEX region and an area of high pressure over eastern China. The cyclone moved northeastward through the AMTEX region, while cold air associated with a following anticyclone moved southeastward over the East China Sea. The track of the cyclone from

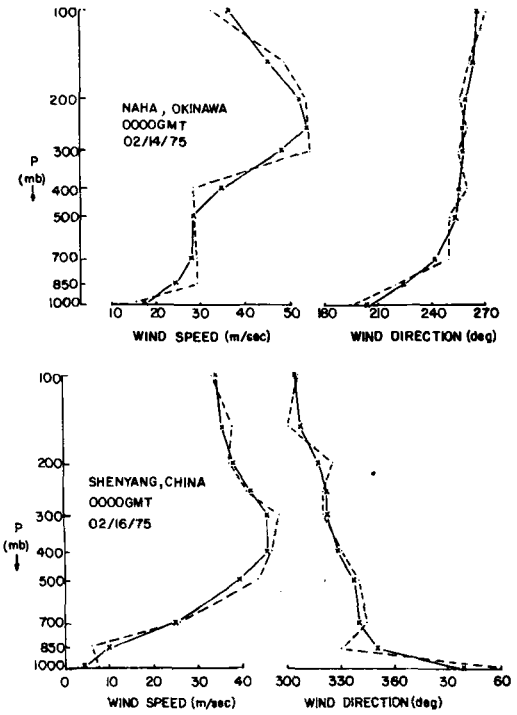

Fig. 2. Vertical profiles of raw (dashed) and vertically filtered (solid) wind speed and direction.

13 to 15 February 1975 is given in Fig. 3. The corresponding surface, 500 mb and 300 mb charts in 24-h intervals from 0000 GMT 13 February to 0000 GMT 16 February are shown in Fig. 4.

The data period began with high pressure dominant throughout most of the region and a frontal zone extending along the southeastern boundary of the computational region. Cyclogenesis occurred on the front just east of Taiwan on 13 February. The low pressure center developed rapidly and was located 300 km north-northwest of Naha, Okinawa at 0000 GMT 14 February. The expanding cyclone system moved rapidly eastward out of the computational region and deepened to 980 mb by 0000 GMT 15 February. During the cyclogenesis a quasi-stationary high pressure center occupied eastern China. After the developing cyclone passed through the AMTEX region, a cold air outbreak occurred over the East China Sea. Satellite cloud photographs reveal that well-organized patterns of mesoscale cellular convection occurred over the East China Sea at 0012 GMT 15 February and persisted for the next two days.

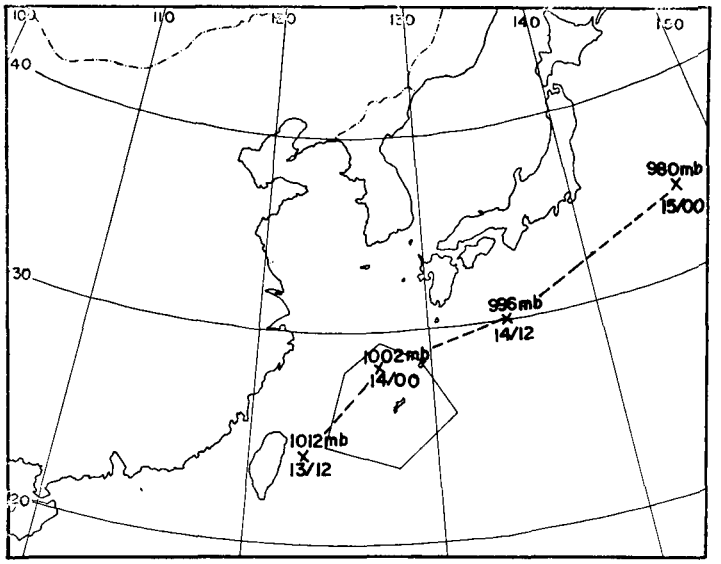

Fig. 3. Cyclone track: 1200 GMT 13 February–0000 GMT 15 February 1975.

As shown in the 500 mb and 300 mb charts, most of the computational region was occupied by a weak upper air ridge when the low level cyclogenesis occurred. On 14 February a short synoptic-scale wave penetrated into eastern China with cold advection evident at 500 mb. This upper air wave moved eastward on 15 February and merged with the longer wave centered north of the computational region. Strong cold air advection occurred at 500 mb over most of the region, particularly over the Yellow Sea and the East China Sea, on 15 and 16 February.

The 300 mb flow was characterized by two jet streams, a southern jet stream extending from southern China eastward through the AMTEX region to south of Japan, and a northern jet stream penetrating from northeastern China through Korea to central Japan. At the beginning of the period these two jet streams were relatively minor features. However, as the upper short wave appeared in the western part of the region, moved eastward, and merged with the longer wave, the two jets increased in intensity.

4. Results

A. *Kinematic fields over the larger region*

Fig. 5 shows the horizontal distribution of absolute vorticity at 500 mb for 0000 GMT each day during the period and the locations of the mesoscale convection cells in the East China Sea. The locations of MCC were determined by referring to satellite cloud photographs within 12 minutes of the last two map times in Fig. 5. The vorticity fields correspond very well with the major features of the 500 mb flow. Comparing Figs. 4 and 5, it is seen that at the beginning of the period the vorticity pattern reflects both the weak upper air ridge dominating much of the region, as well as the southern extent of the cyclonic flow associated with the low center located north of the computational region. On 14 February a well-defined vorticity maximum in excess of 16×10^{-5} s^{-1} occupies eastern China in association with the short synoptic-scale upper wave near the region's western boundary. This center shifts northward in the next 24 hours as the short wave merges with the longer wave pattern centered north of the region. Finally, the vorticity maximum exits the region as the upper trough moves over Japan. On 15 and 16 February MCC occurs in regions of relatively small cyclonic vorticity with negative or near zero vorticity advection.

Fig. 6 depicts horizontal distributions of vertical motion at 500 mb and the areas of greater than 4/8 cloud cover. Also depicted are precipitation and cloud type reports. Cloud and precipitation data were obtained from surface synoptic stations. The vertical motion fields show good agreement

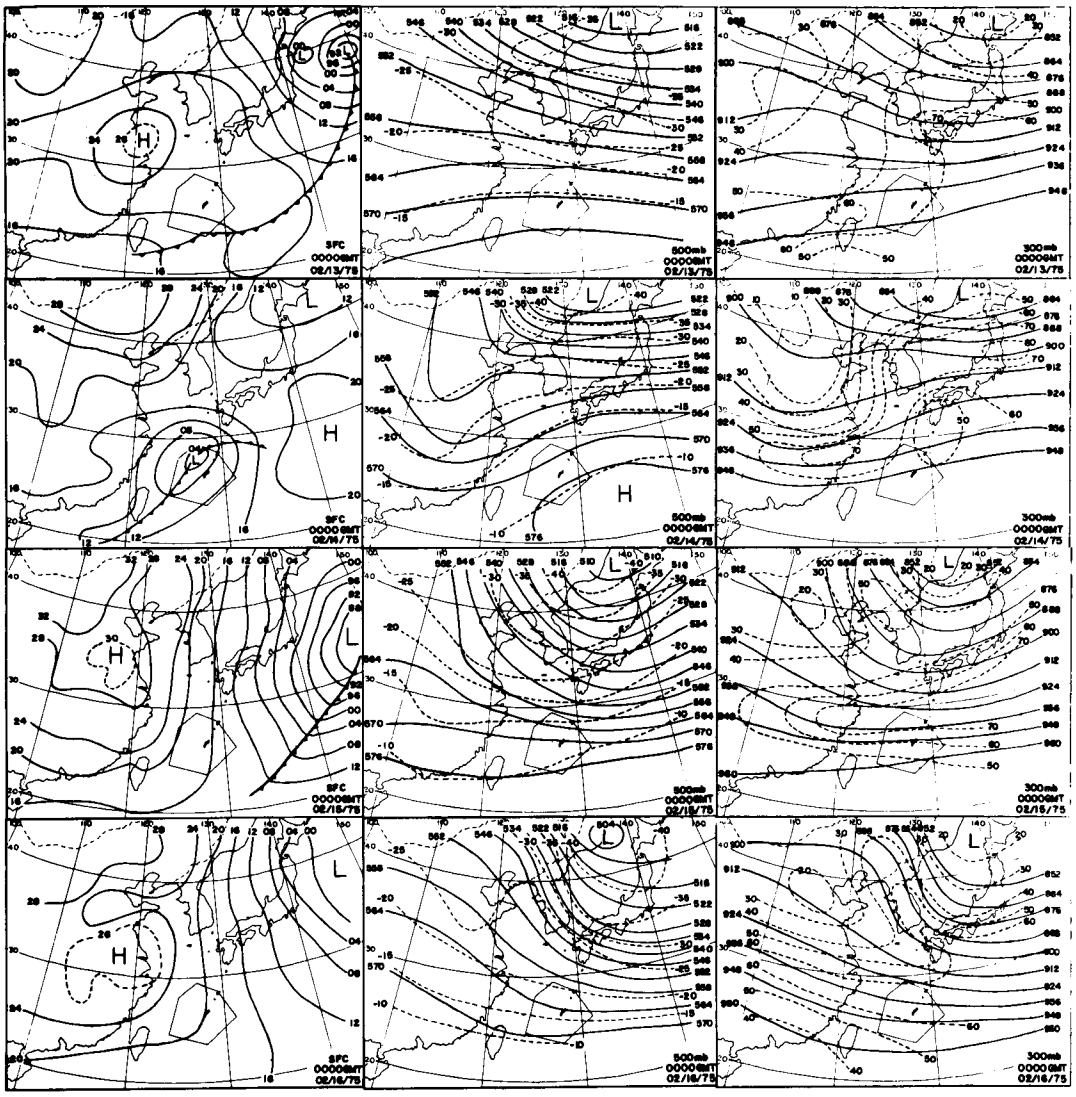

Fig. 4. Sea level isobars in 4 mb increments and surface fronts; 500 mb height contours in 60 m intervals (solid) and temperatures in 5 °C increments (dashed); 300 mb height contours in 120 m intervals (solid) and isotachs in 10 m s^{-1} increments (dashed), 0000 GMT 13 February–0000 GMT 16 February 1975.

with the flow patterns at both the surface and 500 mb (Fig. 4). Upward motion consistently follows the surface low center as it moves northeastward through the AMTEX area, and in general fits the cloud and precipitation regions quite well. Particularly notable is the precipitation with showers, thunderstorms, and cumulonimbus cloud associated with the cyclone on 14 February. It should also be noted, however, that clouds can exist even when the 500 mb vertical motions are downward. This occurs when the clouds result from a circulation feature too small to be captured by the rawinsonde data network, as seen on the 13 February surface map in northern Japan; when the clouds are low stratocumulus, as found on 14 February over eastern China; or when the clouds are cumulus/towering cumulus as seen on 15–16 February over the AMTEX region in association with MCC.

Results depicted in Figs. 5 and 6 compare well

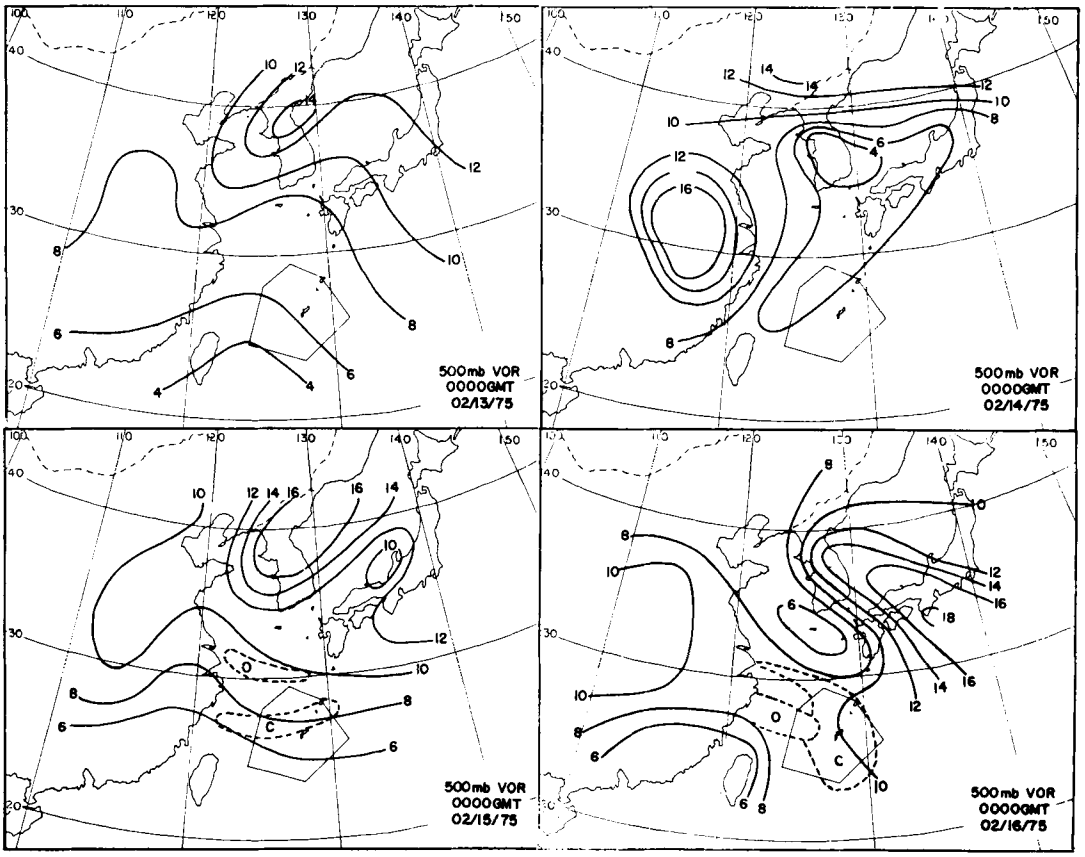

Fig. 5. 500 mb absolute vorticity (solid line) in 2×10^{-5} s^{-1} increments for 0000 GMT 13 February–0000 GMT 16 February 1975. Locations of MCC with C and O representing closed cells and open cells, respectively, are contained within dashed lines.

with computations of the Japan Meteorological Agency (1975). Fig. 7 shows JMA computations of 500 mb relative vorticity and 700 mb vertical motion at 0000 GMT 14 February. Computations were done using the quasi-geostrophic balance and omega equations in a six-level numerical model covering a large portion of eastern Asia and the western Pacific Ocean. The grid interval is 304.8 km at 60° N. Comparing Figs. 5 and 7, both analyses show strong vorticity maxima in eastern China and along the northern boundary of the study area and a vorticity minimum over Korea. Comparing with Fig. 6, areas of upward and downward motion agree quite well. The 500 mb values of the present study exceed the JMA 700 mb values by factors of 2 to 6. Other map times showed similar comparability.

B. *Kinematic fields over the AMTEX region*

In order to understand the characteristic flow features accompanying the MCC, a close examination of the vorticity and vertical motion fields in the AMTEX region is undertaken. All AMTEX region quantities are averages determined from the four computational stations of the AMTEX network previously identified.

Fig. 8 shows the mean time-height cross-section of absolute vorticity and vertical motion for these four stations. The corresponding mean vorticity of the earth ($\bar{f}$) is 6.4×10^{-5} s^{-1}. During the early periods the strong absolute vorticity in the lower troposphere and corresponding weak vorticity in the upper troposphere reveals the developing surface cyclone in the AMTEX region accompanied by the weak upper tropospheric ridge. Later,

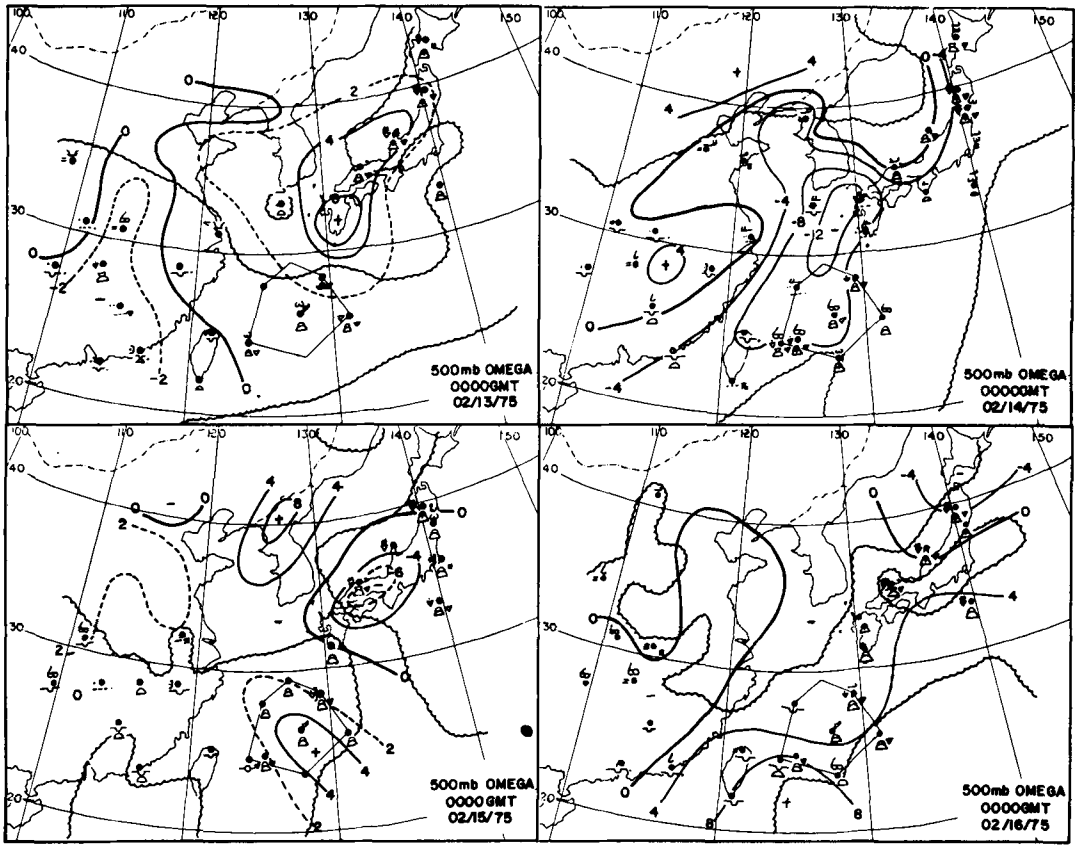

Fig. 6. 500 mb vertical motion (solid lines) in 4 μbar s^{-1} increments, areas of cloud amount greater than 4/8 (scalloped lines), and precipitation/cloud type reports for 0000 GMT 13 February–0000 GMT 16 February 1975.

the maximum vorticity axis moves aloft to the middle troposphere in association with the passage of the upper-air wave, while the surface vorticity diminishes in response to the surface ridge penetration. The vertical motion field shows strong upward motion throughout the troposphere from 1200 GMT 13 February to 1200 GMT 14 February, changing to weaker downward motion in the middle and lower troposphere at later times. Note that the downward motion occurs with cyclonic flow in the middle troposphere. This is consistent with the negative vorticity advection indicated earlier for the AMTEX region (see Fig. 5).

Since the mesoscale convection cells first appeared about 0000 GMT 15 February and remained to the end of the study period, it is possible to conveniently define sub-periods representative of non-MCC and MCC conditions. The non-MCC and MCC periods are defined, respectively, as the periods before and after 0000 GMT 15 February. Thus, a mean non-MCC period quantity is obtained by averaging over the first four 12-h periods, while a mean MCC quantity represents an average over the last three 12-h periods. Fig. 9 shows the vertical profiles of mean absolute vorticity and mean vertical motion for non-MCC and MCC periods in the AMTEX region. Once again the vorticity reflects the cyclonic flow in lower troposphere and anticyclonic flow in upper troposphere during the non-MCC period and the low level ridge penetration during the MCC period. In addition, the MCC period is marked by a change from negative to positive vertical gradient of vorticity in the lower troposphere and an increase in relative vorticity above

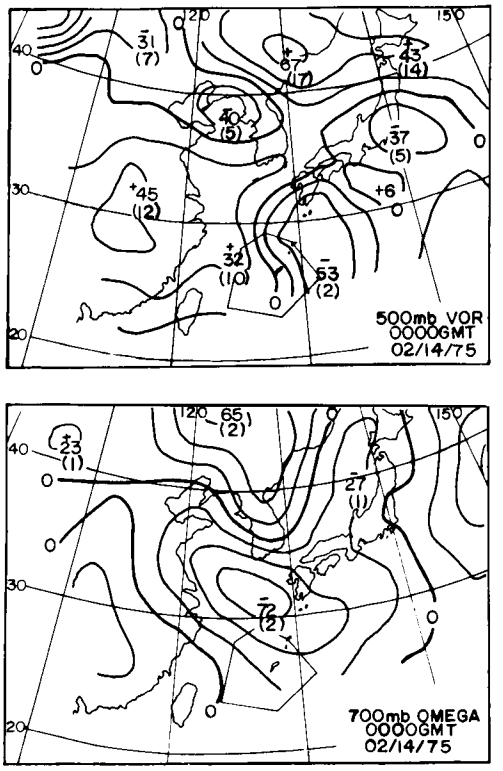

Fig. 7. JMA 500 mb relative vorticity in 20 × 10^{-6} s^{-1} increments and 700 mb vertical motion in 20 × 0.1 mb h^{-1} increments for 0000 GMT 14 February 1975. Maximum/minimum values in parentheses correspond to units of present study; i.e., absolute vorticity in 10^{-5} s^{-1} and vertical motion in μbar s^{-1}.

800 mb. In the vertical motion profile, upward motion dominates in the non-MCC period, while downward motion is characteristic of the MCC period. The latter no doubt provides the mechanism for stabilizing the air above the convecting boundary layer.

5. Summary

Diagnostic analyses of the large-scale vorticity and vertical motions over eastern Asia during a subperiod of AMTEX 75 have been presented.

The onset of mesoscale cellular convection in the East China Sea was preceded by a surface cyclone which developed in conjunction with a short synoptic-scale upper air wave which penetrated the computational region from the western boundary.

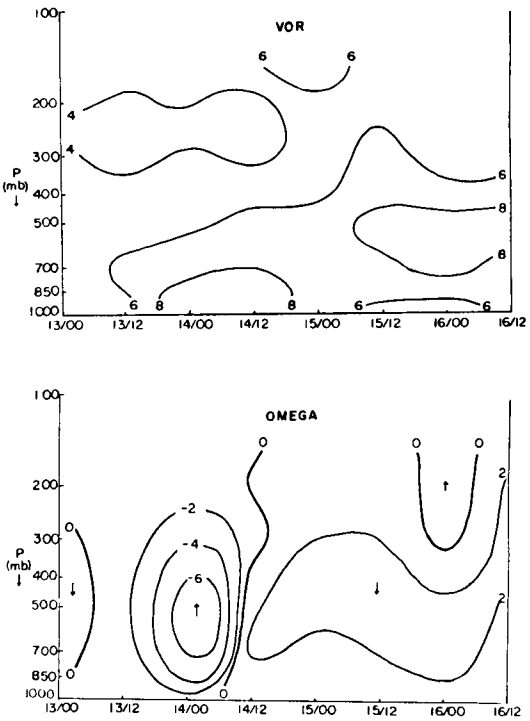

Fig. 8. Time-height cross-section of absolute vorticity (10^{-5} s^{-1}) and vertical motion (μbar s^{-1}) for AMTEX area.

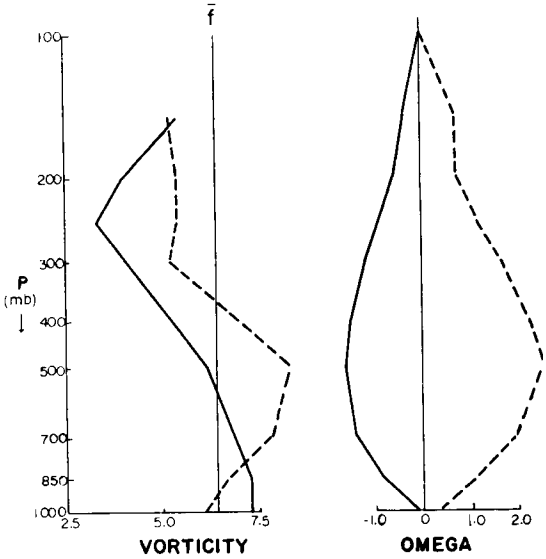

Fig. 9. Mean profile of vertical motion (μbar s^{-1}) and absolute vorticity (10^{-5} s^{-1}) during non-MCC (solid) and MCC (dashed) periods for AMTEX area.

Later the short wave merged with a long wave centered north of the study region as the surface cyclone intensified and expanded. Vertical motion and vorticity fields over the larger computational region correlate well with these large-scale flow features.

In the AMTEX region the transition from the non-MCC to the MCC period is characterized by a shift from upward to downward motion with stronger cyclonic flow in the middle and upper troposphere, and a change from negative to positive vertical gradient of vorticity in the lower troposphere.

6. Acknowledgements

Sincere appreciation is expressed to Ernest M. Agee and Dayton G. Vincent for their advice during the course of this research and to Dr. Agee for the financial support provided through his research project.

Special thanks are due to John H. Ward for his aid in the computational and analysis work, to Barry A. Smith and David W. Allen for their assistance in the preparation of maps and figure drafting, and to Dianne Paro and Kent Cudney for typing the manuscript. This research was sponsored by the Atmospheric Science Section of the National Science Foundation under GARP Grant No. OCD 70-00220 A05.

REFERENCES

Agee, E. M., Chen, T. S. & Dowell, K. E. 1973. A review of mesoscale cellular convection. *Bull. Am. Meteor. Soc. 54*, 1004–1012.

Agee, E. M. & Dowell, K. E. 1974. Observational studies of mesoscale cellular convection. *J. Ap. Meteor. 13*, 46–53.

Chien, H. & Smith, P. J. 1973. On the estimation of kinematic parameters in the atmosphere from radiosonde wind data. *Mon. Wea. Rev. 101*, 252–261.

Danielsen, E. F. 1959. The laminar structure of the atmosphere and its relation to the concept of a tropopause. *Arch. Meteor. Geophys., Bioklim. A11*, 293–332.

Fankhauser, J. C. 1969. Convective processes resolved by a mesoscale rawinsonde network. *J. Ap. Meteor. 8*, 778–798.

Fiedler, F. & Panofsky, H. A. 1970. Atmospheric scales and spectral gaps. *Bull. Am. Meteor. Soc. 51*, 415–423.

Hubert, L. F. 1966. Mesoscale cellular convection. *Meteorological Satellite Laboratory Report*, No. 37, Washington, D.C.

Japan Meteorological Agency, 1975. *AMTEX '75 Data Report vol. 7, Analysis Charts.*

Krishnamurti, T. N. 1968. A study of a developing wave cyclone. *Mon. Wea. Rev. 96*, 208–218.

Krueger, A. F. & Fritz, S. 1961. Cellular cloud patterns revealed by TIROS I. *Tellus 13*, 1–7

Miller, A. & Panofsky, H. A. 1958. Large-scale vertical motions and weather in January 1953. *Bull. Am. Meteor. Soc. 39*, 8–13.

Newton, C. W. & Palmén, E. 1963. Kinematic and thermal properties of a large-amplitude wave in the westerlies. *Tellus 15*, 99–119.

O'Brien, J. J. 1970. Alternative solutions to the classical vertical velocity problem. *J. Appl. Meteor. 9*, 197–203.

O'Neill, T. H. R. 1966. Vertical motion and precipitation computations. *J. App. Meteor. 5*, 595–605.

Schmidt, P. J. & Johnson, D. R. 1972. Use of approximating polynomials to estimate profiles of wind, divergence, and vertical motion. *Mon. Wea. Rev. 100*, 345–353.

Smith, P. J. 1971. An analysis of kinematic vertical motions. *Mon. Wea. Rev. 99*, 715–724.

КИНЕМАТИЧЕСКИЙ АНАЛИЗ АТМОСФЕРЫ НАД ВОСТОЧНОЙ АЗИЕЙ В ТЕЧЕНИЕ ПОДПЕРИОДА "ЭКСПЕРИМЕНТА ПО ТРАНСФОРМАЦИИ ВОЗДУШНЫХ МАСС—1975".

В работе исследуются поля крупномасштабных завихренности и вертикальных движений над восточной Азией в течение подпериода (13–16 февраля) "Эксперимента по трансформации воздушных масс—1975" (АМТЭКС). Это был период циклогенеза и последующего образования мезомасштабной ячейковой конвекции (МЯК) над областью АМТЭКС.

Поля вертикальных движений и завихренности отражают развитие циклона и короткую волну синоптического масштаба, распространяющуюся через область расчета. Результаты для области АМТЭКС показывают, что в течение МЯК в нижней тропосфере могут происходить крупномасштабные нисходящие движения и изменения от отрицательных к положительным вертикальным градиентам завихренности.